Available online at www.sciencedirect.com

ScienceDirect

Procedia Engineering 114 (2015) 658 – 666

Procedia Engineering

www.elsevier.com/locate/procedia

1st International Conference on Structural Integrity

Microstructure Evolution, Tensile Properties, and Fatigue Damage Mechanisms in Ti-6Al-4V Alloys Fabricated by Two Additive Manufacturing Techniques

Yuwei Zhai[a,]*, Haize Galarraga[a], and Diana A. Lados[a]

[a]*Worcester Polytechnic Institute, Integrative Materials Design Center, 100 Institute Road, Worcester, MA 01609, USA*

Abstract

Additive Manufacturing (AM) technology is capable of building 3D near-net-shaped functional parts directly from computer models, using unit materials, such as powder or wire. AM offers superior geometrical flexibility with significantly reduced manufacturing lead time, energy, and material waste. These benefits make AM desirable for critical transportation applications, providing that structural integrity and performance requirements are met or exceeded. In this study, structural materials fabricated by two AM techniques were investigated: Laser Engineered Net Shaping (LENS) and Electron Beam Melting (EBM). Ti-6Al-4V alloys were produced using both methods and various processing conditions, which resulted in different microstructures and mechanical properties given their unique thermal histories. Characteristic microstructures were determined for all cases. Room temperature tensile and fatigue crack growth (FCG) properties were also evaluated and compared in different orientations with respect to the deposition direction. The effects of post-deposition heat treatment on tensile and FCG properties were determined. The results are systematically presented and discussed from both the material/process optimization, as well as structural design and fatigue life prediction perspectives.

Peer-review under responsibility of INEGI - Institute of Science and Innovation in Mechanical and Industrial Engineering

Keywords: Ti-6Al-4V, Microstructure evolution, Mechanial properties, Fatigue damage mechanisms, Laser engineered net shaping, Electron beam melting

* Corresponding author. Tel.: +1-508-831-5255.
E-mail address: yzhai@wpi.edu

Peer-review under responsibility of INEGI - Institute of Science and Innovation in Mechanical and Industrial Engineering
doi:10.1016/j.proeng.2015.08.007

1. Introduction and background

Additive Manufacturing (AM) technology represents a family of advanced near-net-shaping techniques that are able to build 3D geometries directly from computer models, using material units, most commonly powder and wire. Although various AM techniques were developed, their working principles can be generalized [1]. Standardized definition and terminologies were also developed specifically for AM (ASTM F2792-12a). Researches have been done to study the microstructures and tensile properties in AM-fabricated materials [2-10]. However, the materials' performances under cyclic loading, i.e., fatigue properties were rarely reported [11], neither was there a systematic comparison between microstructures and properties obtained using different AM techniques.

In this study, two AM techniques, Laser Engineered Net Shaping (LENS) and Electron Beam Melting (EBM) were studied and compared using Ti-6Al-4V alloys. Systematic investigation of the influence of processing parameters on microstructure evolution, tensile properties, and fatigue properties were performed. The effects of post-deposition heat treatments were also studied.

LENS technique was originally developed at Sandia National Laboratories and was commercialized by Optomec, Inc. in 1997 [12]. In the same year, the Swedish company ARCAM AB was founded, and published its first patent for EBM technique in 2001 [13]. Schematic representations illustrating the working principles of LENS and EBM are shown in Fig. 1 [1]. During LENS process, the laser beam creates a melting pool on a substrate placed onto the x-y table, material powder is then injected into the melting pool to fuse and solidify into a bead. At the same time, the substrate moves with the x-y table (in x-y directions), enabling the selective deposition of one layer. Then, the laser beam and material deposition head move together upward (in z direction) to start the deposition of the second layer. This procedure is repeated until a 3D geometry is completed. The finished geometry and the substrate can be separated by machining (apart from the cases where the process is applied for repairing). During EBM process, material powder is provided by powder hoppers instead, and is uniformly distributed in one layer on the build platform by a rake. Powder in this layer is then selectively melted by the electron beam. After the first layer is completed, the build platform lowers, allowing a new layer of powder to be uniformly distributed on top of the first layer. This new layer of powder is again selectively melted by the electron beam, and the process continues until the complete 3D geometry is built. The finished geometry is freed by blasting off the excess powder, which is usually partially recycled.

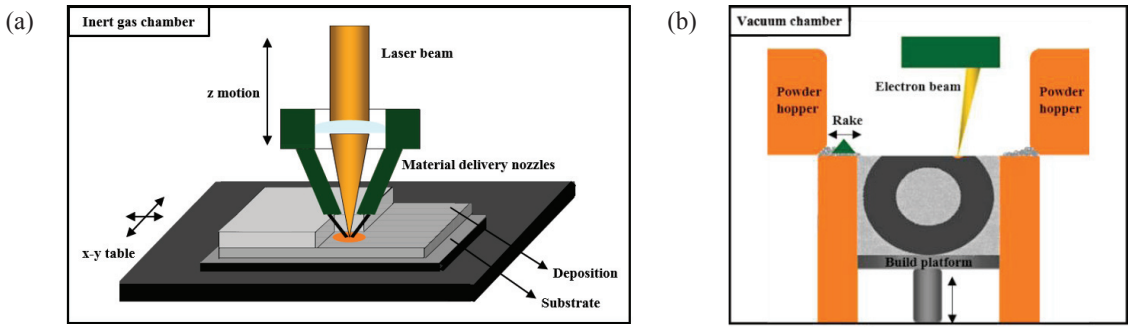

Fig. 1. Working principles of (a) LENS [1]; (b) EBM.

2. Experimental procedure

2.1. Powder precursors and sample fabrication

Spherical gas atomized (GA) Ti-6Al-4V powder is used in both LENS and EBM fabrications, Fig. 2. Particle sizes are similar for the two techniques. The powder used in EBM, Fig. 2(b), contains 50% recycled powder [14].

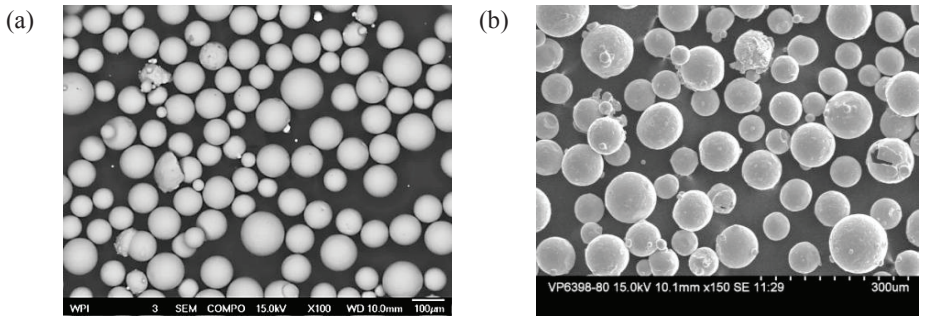

Fig. 2 Powder precursors used in (a) LENS and (b) EBM fabrication [14].

LENS samples were fabricated at Benét Laboratories, using an Optomec L850-R system. Two sets of processing parameters were applied, Table 1.

Table 1. LENS processing parameters.

	Low power (LP)	High power (HP)
Laser power (W)	330	780
Powder feed rate (g/min)	1.0	2.0
Layer thickness (mm)	0.3	0.4
Hatch spacing (mm)	0.5	1.0
Deposition speed (m/min)	0.6	0.8

Near-net-shaped rectangular depositions were built on top of mill-annealed Ti-6Al-4V plates (substrate). The geometries of the depositions were designed for the convenience of extracting tensile specimens, Fig. 3(a, b), and fatigue specimens, Fig. 3(c, d). Post-LENS annealing was also performed to generate comparison with the as-deposited cases. The annealing treatment used was: 760°C +/- 4°C for 1 hour in vacuum, followed by air cooling.

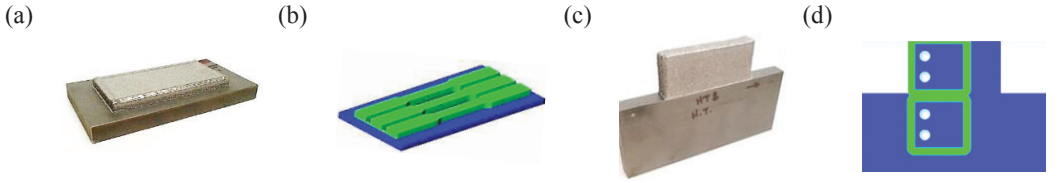

Fig. 3. LENS samples preparation: (a) near-net-shaped deposition for tensile tests; (b) extraction of tensile specimens; (c) near-net-shaped deposition for fatigue tests; (d) extraction of fatigue specimens (top: from bulk deposition; bottom: from substrate).

EBM samples were fabricated at Oak Ridge National Laboratory (ORNL) in two batches, B1 and B2, representing two different machine models A2 and Q10. The processing parameters were defined by the internal algorithm of the ARCAM machines. Similarly, near-net-shaped cylindrical and rectangular samples were designed for tensile and fatigue crack growth studies respectively, Fig. 4(a, b). The effects of solutionizing, annealing temperature and time, and aging temperature and time have been systematically evaluated for EBM fabricated Ti-6Al-4V [14], and the optimum heat treatment was used in this study: solutionizing at 950°C for 1 hour, water quenching to room temperature; aging at 500°C for 7 hours, and air cooling.

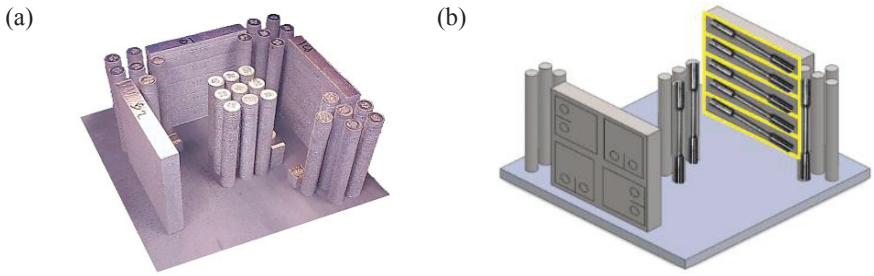

Fig. 4. EBM samples preparation: (a) near-net-shaped rectangular and round samples; (b) extraction of fatigue and tensile specimens.

2.2. Microstructure analysis and mechanical testing

Metallographic samples were mounted in Bakelite and polished using diamond suspension down to 0.05µm. Samples were then etched by Kroll's reagent (2% HF, 6% HNO_3 and 92% DI H_2O). The microstructures were characterized using Nikon's MA 200 Eclipse optical microscope with Elements-D image analysis software.

Rectangular or round tensile bars were machined per ASTM E8, with a gage length of 25 mm. Room temperature tensile tests were conducted using an Instron universal testing machine, at a strain rate of 1.3 mm/min.

Fatigue crack growth (FCG) experiments were performed using compact tension specimens machined per ASTM E647. Overall specimen dimensions were 39 mm × 38 mm × 6 mm. The initial notch was introduced by electrical discharge machining (EDM), using a wire thickness of 0.25 mm. The initial notch length (measured from the pin holes) was 25 mm. Constant stress ratio tests at R=0.1 were performed at room temperature in lab air, with a relative humidity of 20-50%. The tests were run under K-control at a cyclic frequency of 20 Hz in order to generate data in Regions I and II. Specifically, a K-gradient of -0.2/mm was used for the decreasing K part of the test to determine the crack growth threshold value, ΔK_{th}. Region II data were generated under increasing K tests with a K-gradient of +0.2/mm. The final part of the tests was run at constant load at a cyclic frequency of 5 Hz to generate data in Region III of fast crack growth. Generated FCG data were then analyzed using FTA Automated FCG Analysis software and plotted in Grapher. To establish the FCG damage mechanisms, one half of the fractured compact tension specimens was vertically sectioned through the middle of the thickness and then metallographically prepared for two dimensional examination of the crack path. The other half was used for examinations of the fracture surfaces, using a JEOL-7000F scanning electron microscope (SEM).

3. Results and discussion

3.1. Microstrucutre characterization

3.1.1. LENS fabricated Ti-6Al-4V

Panoramic images of the entire depositions were taken at low magnification for LP and HP cases, Figs. 5(a, b). Directional columnar β grains were found dominant as a result of heat extraction from the substrate; deposition-substrate interfaces (macro-HAZ) were observed as a result of partial melting of the substrate; layer bands could also be seen after etching, due to microstructure coarsening at the layer boundaries (micro-HAZ) from remelting of previous layers. Wider macro-HAZ (~800µm) and thicker layers (600-900µm) were observed in HP fabrication, Fig. 6(a), than in LP fabrication (~500µm macro-HAZ, and 300-800µm layer thickness), Fig. 6(b) [1].

At high magnification, LP fabricated Ti-6Al-4V showed martensitic microstructure with acicular α' phases (~0.6µm thick), Fig. 5(c); while HP fabricated Ti-6Al-4V showed regions of parallel α lath (~1.7µm thick), and regions of acicular α' phases, leading to a mixed microstructure of α' + α in prior β matrix, Fig. 5(d). At the prior β boundaries, 1-2µm thick α layers were observed in HP case but not in LP case, Figs. 5(c, d), indicating slower cooling during HP fabrication than LP fabrication. Substrate material was mill-annealed Ti-6Al-4V, with a typical microstructure of equiaxed α phases in β matrix, Fig. 5(e).

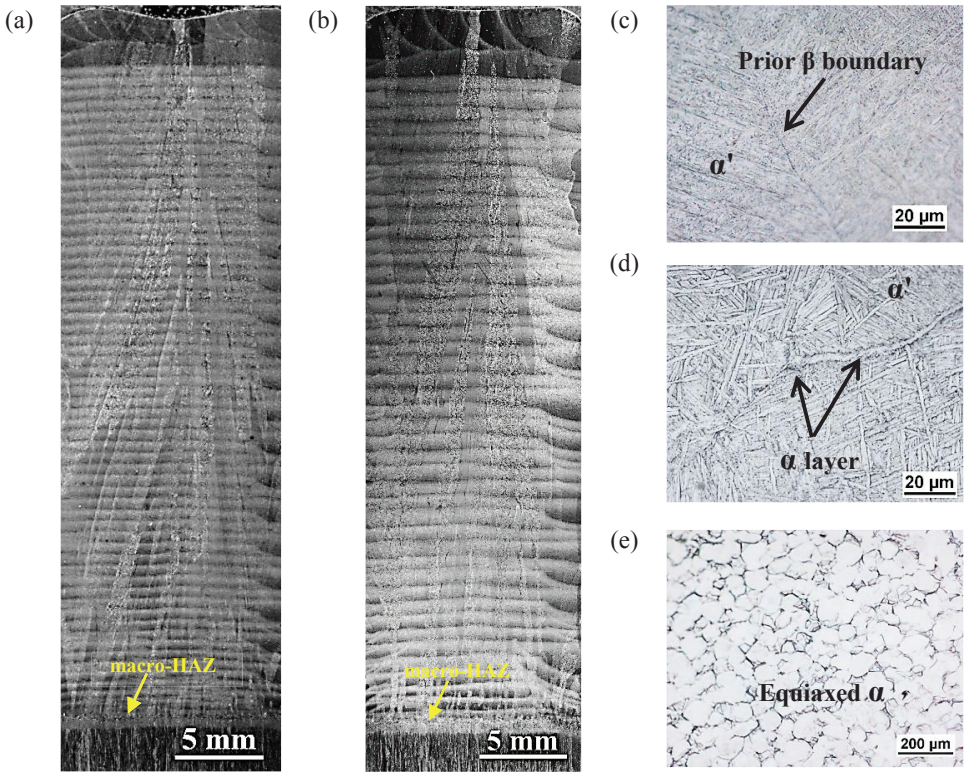

Fig. 5. Microstructures of LENS faricated Ti-6Al-4V: (a) LP fabrication; (b) HP fabrication; (c) acicular α' phases in LP fabricated Ti-6Al-4V; (d) mixture of α' and α in HP fabricated Ti-6Al-4V; (e) mill-annealed substrate.

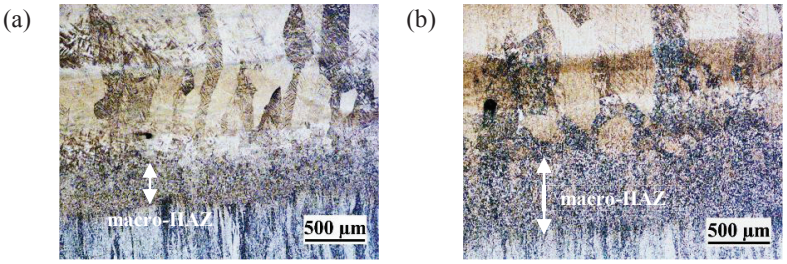

Fig. 6. Macro-HAZ and layer thickness in: (a) LENS LP and (b) LENS HP fabrication.

3.1.2. EBM fabricated Ti-6Al-4V

Columnar β grains were also found in EBM fabricated Ti-6Al-4V for both B1 and B2 batches, Figs. 7(a, b). Different from LENS fabrication which is typical of fast cooling, in EBM, the powder bed was held at 650-750°C through out the process, and was slowly cooled to room temperature when fabrication completed. Long period exposure under 650-750°C decomposed all the α' phases formed during solidification; and since the minimum cooling rate required to form martenstic microstructure in Ti-6Al-4V is 410°C/s [15], the slow cooling upon fabrication completion did not lead to any martensitic formation. The resulting microstrucure in EBM fabricated Ti-6Al-4V was found to be fine α + β lamellae, Figs. 7(c, d).

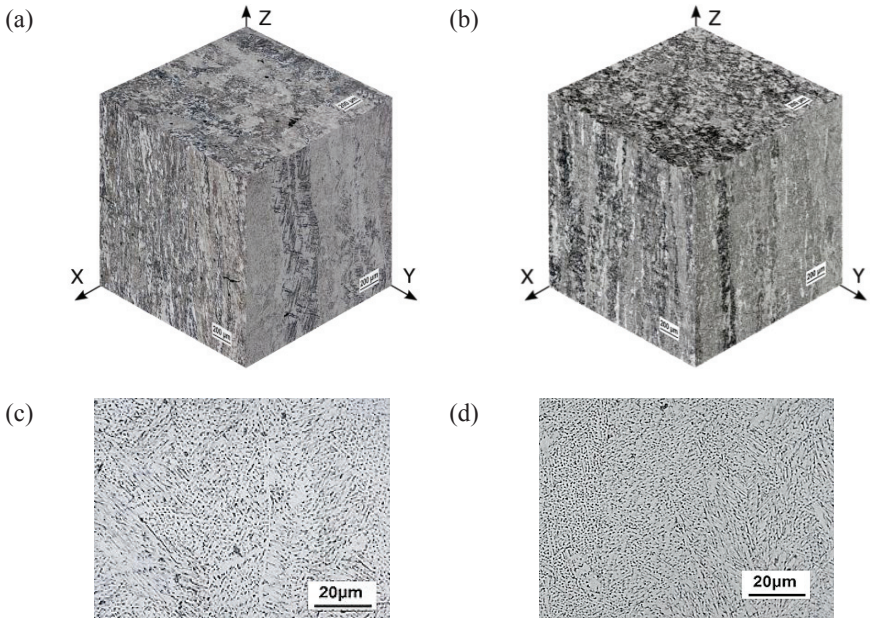

Fig. 7. Microstructures of EBM faricated Ti-6Al-4V: (a, c) B1; (b, d) B2.

3.2. Room temperature tensile properties and the influences of post-deposition heat treatments

3.2.1. LENS fabricated Ti-6Al-4V

For LENS farbication, tensile tests were conducted only at horizontal orientation, Fig. 3(b). Tensile properties of LENS fabricated Ti-6Al-4V and a comparison with mill-annealed Ti-6Al-4V (substrate) are provided in Table 2. In general, the yield strength and ultimate tensile strength of LENS depositions are higher than those of the mill-annealed substrate. Comparing between LENS fabrications, LP as-deposited Ti-6Al-4V yieled higher strength, but significantly lower ductility due to the presence of α' martensite. After annealing, significant increase in ductility was observed as a result of α' decomposition into α + β lamellae. Similar heat treating effect was also found in HP fabricated Ti-6Al-4V alloys, as the elongation increased from 7% to 10% after annealing.

Table 2. Room temperature tensile properties of LENS fabricated Ti-6Al-4V.

	YS (MPa)	UTS (MPa)	%EL
LP as deposited	1005	1103	4
LP annealed	1000	1073	9
HP as deposited	990	1042	7
HP annealed	991	1044	10
Substrate (mill-annealed)	970	1030	16

3.2.2. *EBM fabricated Ti-6Al-4V*

For EBM fabrication, tensile tests were conducted at both horizontal and vertical orientations, Fig. 4(b). Tensile data for EBM fabricated Ti-6Al-4V are given in Table 3. Similar tensile properties were found in as-deposited B1 and B2 batches at two diffrernt orientations. Comparing these results with the as-deposited cases in LENS fabrication, EBM and LENS yielded comparable tensile strength, but EBM fabrication achieved much better

ductility than LENS fabrication due to the powder bed heating, which prevents the formation of martensitic α' phases. The optimum post-EBM heat treatment was found to be able to further increase the tensile strength while maintaining a moderate ductility.

Table 3. Room temperature tensile properties of EBM fabricated Ti-6Al-4V.

	YS (MPa)	UTS (MPa)	%EL
B1-horizontal as deposited	1006	1066	15
B1-vertical as deposited	1001	1073	11
B2-horizontal as deposited	973	1032	12
B2-vertical as deposited	1051	1116	15
Solutionized and aged	1039	1294	10

3.3. Fatigue crack growth (FCG) properties and mechanisms

For both LENS and EBM fabrications, FCG tests were conducted at two orientations: horizontal and vertical. An illustration of the compact tension specimens showing crack growth directions (arrows) with respect to the deposition direction (D) and columnar grains are shown in Fig. 8.

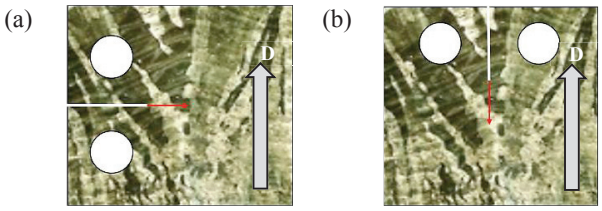

Fig. 8. Fatigue crack propagation directions (arrows) with respect to the deposition directions (D) and columnar grains: (a) horizontal propagation; (b) vertical propagation.

3.3.1. FCG properties

Experimentally measured FCG data of LENS and EBM fabricated Ti-6Al-4V are shown in Fig. 9. For LENS horizontal propagation cases, Fig. 9(a), LENS fabricated Ti-6Al-4V alloys in general showed lower threshold value $\Delta \boldsymbol{K_{th}}$ but higher fracture toughness $\Delta \boldsymbol{K_{FT}}$ than mill-annealed Ti-6Al-4V (substrate), indicating a better high cycle fatigue performance in mill-annealed Ti-6Al-4V, and a better low cycle fatigue performance in LENS Ti-6Al-4V. Comparisons between LENS fabricated alloys indicated that LP fabrication yielded slightly lower threshold value than HP fabrication due to the presence of martensitic α' phases. After annealing, slight increase in $\Delta \boldsymbol{K_{th}}$ was found in LP fabricated Ti-6Al-4V as a result of α' decomposition. Similar observations were found in vertical propagation cases, Fig. 9(b).

In EBM fabricated Ti-6Al-4V alloys, B1 and B2 bactches showed similar threshold and toughness values for both horizontal and vertical propagation directions, thus only data from B2 batch are plotted here in Fig. 9(c) against the heat treated conditons. Compared to LENS, EBM as-deposited alloys showed similar threshold to LENS HP fabricated alloys, i.e. higher threshold than LENS LP fabricated alloys, due to their similar microstructures. Fracture toughness values in as-deposited EBM Ti-6Al-4V alloys are comparable to those in LENS. After solutionizing and aging, significant increase in threshold was found in vertical propagation direction, achieving a threshold value comparable to the mill-annealed Ti-6Al-4V; while significant increase in fracture toughness was found in horizontal propagation direction.

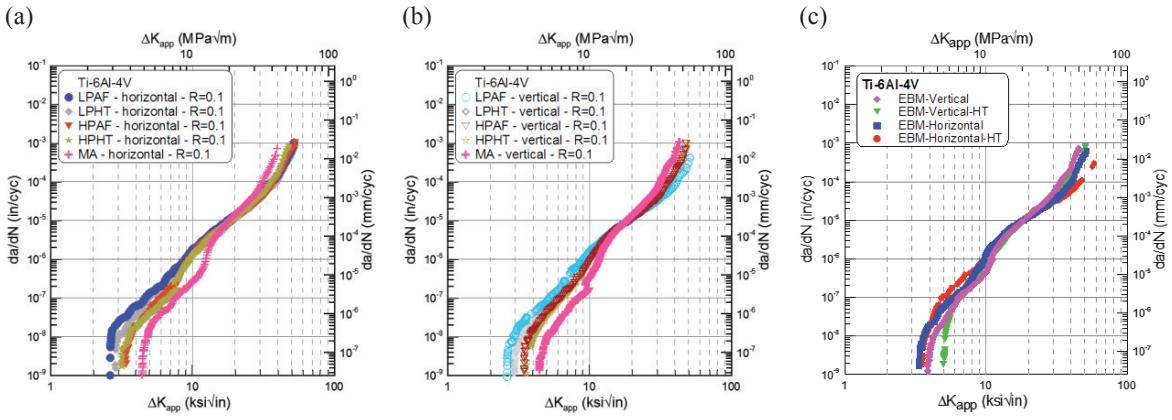

Fig. 9. FCG data of: (a) LENS fabricated Ti-6Al-4V at horizontal fatigue crack propagation direction; (b) LENS fabricated Ti-6Al-4V at vertical fatigue crack propagation direction; (c) EBM fabricated Ti-6Al-4V.

3.3.2. FCG mechanisms

The microstructures of LENS and EBM fabricated Ti-6Al-4V all contain columnar β grains, and very fine α morphologies (acicular α' in LENS LP; α' with α + β lamellae in LENS HP; α + β lamellae in EBM). This similarity yielded comparable FCG mechanisms in both materials. Crack growth side profiles at various ΔK levels and propagation regimes (i.e. threshold, Region II and Region III) for LENS, EBM and mill-annealed Ti-6Al-4V are shown in Fig. 10. Crack interaction with α'/α phases was found to be the primary propagation mechanism in LENS fabricated Ti-6Al-4V, and crack interaction with α lath and colonies controlled the crack growth in EBM fabricated Ti-6Al-4V. In mill-annealed Ti-6Al-4V, crack interaction with equiaxed α phases was found in Region I, and interacion with β phases instead was found in Region III.

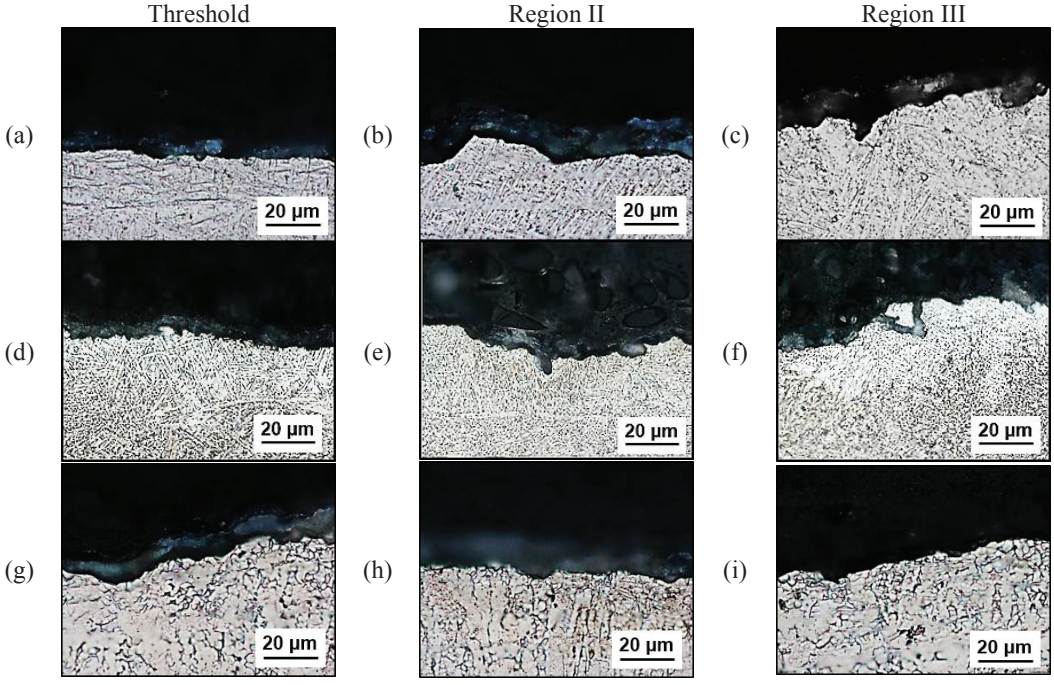

Fig. 10. FCG mechanisms in: (a, b, c) LENS; (d, e, f) EBM; (g, h, i) mill-annealed Ti-6Al-4V at different ΔK levels.

4. Conclusions

i. The microstructures of LENS and EBM fabricated Ti-6Al-4V all showed directional columnar prior β grains parallel to the deposition directions.
ii. The α morphology in LENS LP fabricated Ti-6Al-4V is acicular α', indicating martensitic transformation; while in HP fabricated alloys, both areas of fine α + β lamellae and α' were observed, indicating a slower cooling rate in HP fabrication.
iii. Post-LENS annealing at 760°C decomposes α' phases, and thus increases material's ductility.
iv. The α morphology in EBM fabrication consists of fine α + β lamellae.
v. EBM fabricated Ti-6Al-4V yielded comparable tensile strength but significantly higher ductility than LENS fabricated Ti-6Al-4V due to the absence of martensitic phases.
vi. LENS fabrication yielded better low cycle fatigue performance, but poorer high cycle fatigue performance than mill-annealed Ti-6Al-4V.
vii. LENS HP fabrication yielded higher FCG threshold values in Ti-6Al-4V than LP fabrication; EBM as-deposited Ti-6Al-4V have comparable threshold values to LENS HP cases.
viii. Fracture toughness values are comparable between LENS and EBM fabrication.
ix. For EBM fabricated Ti-6Al-4V, solutionizing and aging treatment significantly increased threshold value and fracture toughness in vertical and horizontal propagation directions respectively.
x. FCG mechanisms were correlated primarily with α/α' phases and colonies in both LENS and EBM fabricated Ti-6Al-4V; in mill-annealed Ti-6Al-4V, the mechanism changes from interacting with α phases in Region I, to interacting with β phases in Region III.

References

[1] Y. Zhai, D.A. Lados, J.L. LaGoy, Additive manufacturing: making imagination the major limitation, JOM 66 (5) (2014) 808-816.
[2] L.E. Murr, E.V. Esquivel, S.A. Quinones, S.M. Gaytan, M.I. Lopez, E.Y. Martinez, F. Medina, D.H. Hernandez, E. Martinez, J.L. Martinez, S.W. Stafford, D.K. Brown, T. Hoppe, W. Meyers, U. Lindhe, R.B. Wicker, Microstructures and mechanical properties of electron beam-rapid manufactured Ti–6Al–4V biomedical prototypes compared to wrought Ti–6Al–4V, Materials Characterization, 60 (2) (2009) 96-105.
[3] M.L. Griffith, M.T. Ensz, J.D. Puskar, C.V. Robino, J.A. Brooks, J.A. Philliber, J.E. Smugeresky and W.H. Hofmeister, Understanding the Microstructure and Properties of Components Fabricated by Laser Engineered Net Shaping (LENS), MRS Proceedings, 625 (2000) 9-20.
[4] F. Wang, J. Mei, Xinhua Wu, Microstructure study of direct laser fabricated Ti alloys using powder and wire, Applied Surface Science 253 (3) (2006) 1424-1430.
[5] X. Wu, J. Mei, Near net shape manufacturing of components using direct laser fabrication technology, Journal of Material Processing Technology 135 (2003) 266−270.
[6] X. Wu, J. Liang, J. Mei, C. Mitchell, P.S. Goodwin, W. Voice, Microstructures of laser-deposited Ti−6Al−4V, Material & Design, 25 (2004) 137-144.
[7] L. Qian, J. Mei, J. Liang, X. Wu, Influence of position and laser power on thermal history and microstructure of direct laser fabricated Ti−6Al−4V samples, Material Science and Technology 21 (2005) 597−605.
[8] J. Gockel, J. Beuth, K. Taminger, Integrated control of solidification microstructure and melt pool dimensions in electron beam wire feed additive manufacturing of Ti-6Al-4V, Additive Manufacturing, 1–4 (2014) 119-126.
[9] L. Facchini, E. Magalini, P. Robotti, A. Molinari, Microstructure and mechanical properties of Ti-6Al-4V produced by electron beam melting of pre-alloyed powders, Rapid Prototyping Journal 15 (3) (2009) 171-178.
[10] L.E. Murr, E.V. Esquivel, S.A. Quinones, S.M. Gaytan, M.I. Lopez, E.Y. Martinez, F. Medina, D.H. Hernandez, E. Martinez, J.L. Martinez, S.W. Stafford, D.K. Brown, T. Hoppe, W. Meyers, U. Lindhe, R.B. Wicker, Microstructures and mechanical properties of electron beam-rapid manufactured Ti–6Al–4V biomedical prototypes compared to wrought Ti–6Al–4V, Materials Characterization 60 (2) (2009) 96-105.
[11] S. Leuders, M. Thöne, A. Riemer, T. Niendorf, T. Tröster, H.A. Richard, H.J. Maier, On the mechanical behaviour of titanium alloy TiAl6V4 manufactured by selective laser melting: Fatigue resistance and crack growth performance, International Journal of Fatigue 48 (2013) 300-307.
[12] R.R. Mudge, N.R. Wald, Laser engineered net shaping advances additive manufacturing and repair, Welding Journal 86 (1) (2007) 44-48.
[13] L.E. Andersson, M. Larsson, Device and arrangement for producing a three-dimensional object, Patent WO 2001081031 A1.
[14] H. Galarraga, D. Lados, Microstructure, static and dynamic properties, and damage mechanisms, and ICME in Ti-6Al-4V fabricated by electron beam melting, iMdc internal report, 2015.
[15] G. Lütjering, J.C. Williams, Titanium, Springer Berlin Heidelberg, 2003.